Cryogenic Photochemical Synthesis and Electronic Spectroscopy of Cyanotetracetylene

Urszula Szczepaniak, Robert Kolos, Marcin Gronowski, Michèle Chevalier, Jean-Claude Guillemin, Michal Turowski, Thomas Custer, Claudine Crépin

Cryogenic Photochemical Synthesis and Electronic Spectroscopy of Cyanotetracetylene

Urszula Szczepaniak[a, b] *, *Robert Kołos*[b], *Marcin Gronowski*[b], *Michèle Chevalier*[a], *Jean-Claude Guillemin*[c], *Michał Turowski*[b, †], *Thomas Custer*[b], *and Claudine Crépin*[a]

[a] Institut des Sciences Moléculaires d'Orsay (ISMO), CNRS, Univ. Paris-Sud, Université Paris-Saclay, F-91405 Orsay, France,

[b] Institute of Physical Chemistry, Polish Academy of Sciences, Kasprzaka 44/52, 01-224 Warsaw, Poland,

[c] Institut des Sciences Chimiques de Rennes, École Nationale Supérieure de Chimie de Rennes, CNRS, UMR 6226, 11 Allée de Beaulieu, CS 50837, 35708 Rennes Cedex 7, France

[*] *tel. +48 22 343 3353 ; e-mail : uszczepaniak@ichf.edu.pl, urszula.szczepaniak@u-psud.fr*

Present addresses

† University of Colorado at Boulder, Department of Chemistry and Biochemistry, 215 UCB, Boulder, CO 80309-0215

ABSTRACT

HC_9N is a molecule of astrochemical interest. In this study, it was produced in cryogenic Ar and Kr matrices from UV-photolyzed diacetylene/cyanodiacetylene mixtures. Its strong phosphorescence was discovered and served for the identification of the compound. Vibrationally-resolved phosphorescence excitation spectra gave insight into excited singlet electronic states. Two electronic systems were observed: around 26 000 – 34 000 cm^{-1} and 35 000 – 50 000 cm^{-1}. Energies of the second excited singlet and the lowest triplet state were derived from analysis of these systems. Vibrational and electronic spectroscopic features were assigned with the assistance of density functional theory calculations. Some trends concerning the electronic spectroscopy of $HC_{2n+1}N$ family molecules are presented.

INTRODUCTION

Monocyanopolyynes ($HC_{2n+1}N$) constitute the most prominent homologous series of astrochemically-relevant molecules. They have been detected via microwave rotational transitions in many extraterrestrial sources up to n = 4. Cyanoacetylene, HC_3N, the smallest neutral molecule possessing both –C≡C– and –C≡N structural motifs, was first observed in a star-forming region Sagittarius (Sgr B2(N))[1] and then in other Galactic[2–4] and extragalactic[5] radio sources. It has also been detected in the atmosphere of Titan[6,7] and in Hale-Bopp comet[8]. Along with cyanoacetylene, longer members of the $HC_{2n+1}N$ series (n = 2, 3) have been found in several molecular clouds.[9] HC_9N (cyanotetraacetylene, 1-cyano-octa-1,3,5,7-tetrayne or nona-2,4,6,8-tetraynenitrile) was first observed in 1978 at millimeter wavelengths in the dense interstellar cloud HCl-2.[10] It has also been found in expanding circumstellar envelopes (IRC +10216 [11,12] and CRL 2688 [12]). As observations of the n = 5 species, $HC_{11}N$, in IRC +10216 [13] and in the Taurus Molecular Cloud[14] have been challenged, first in IRC +10216 [14] and now in TMC-1,[15] HC_9N is currently considered the longest member of the family to have been observed in space.

The astrochemical synthesis of monocyanopolyynes probably involves the reactions of $CN^{\bullet}$ or $C_{2n+1}N^{\bullet}$ radicals with polyynic hydrocarbons $HC_{2m}H$. Cherchneff *et al.* proposed the following pathway for formation of monocyanopolyynes around IRC +10216: $HC_2H + C_{2n+1}N^{\bullet} \rightarrow HC_{2n+3}N + H^{\bullet}$[16,17]. Loomis *et al.*[15] suggested that cyclization reactions are responsible for non-detection of n >4 cyanopolyynes.

The astronomical detections of HC_9N were based on microwave spectroscopy combined with quantum chemical studies of molecular structure.[18–21] Density functional theory (B3LYP) investigations[22] have suggested that $HC_{2n+1}N$ compounds should be linear and polyynic (having alternating single and triple bonds) at least up to n = 8. Vichietti and Haiduke predicted IR spectra of long cyano-[23] ($HC_{2n}CN$) and isocyanopolyynes[24] ($HC_{2n}NC$) and suggest that the central triple bond stretching mode is the one producing the strongest band.

Gas-phase spectroscopic studies of HC_9N are limited to microwave measurements in which minute amounts of the substance are transiently formed in a discharge plasma using acetylene with acrylonitrile[25] or dicyanoacetylene with cyanoacetylene[26] as seed gases. These investigations allowed derivation of the molecular geometry. Independently, electronic absorption and NMR spectra of HC_9N in organic solvents have been reported [27–32]. In particular, Wakabayashi *et al.*[31] obtained $HC_{2n+1}N$ (n = 3-6) by laser ablation of isotope-enriched (99 % ^{13}C) graphite in liquid acetonitrile followed by chromatographic purification. Very small amounts of the compound were then characterized by UV absorption and NMR spectroscopy. Isotopic experiments proved that the carbon atoms of HC_9N came both from graphite and solvent. The molecule has also appeared among the products of graphite bombardment with high energy H_2 and N_2 beams.[33]

In order to extend the spectroscopic characterization of cyanotetraacetylene, we aimed at synthesizing the molecule in noble gas matrices. Cryogenic photochemical syntheses of cyanopolyacetylenes have already been demonstrated for cyanodiacetylene (HC_5N)[34,35] and cyanotriacetylene (HC_7N)[36]. Cyanodiacetylene appeared in solid Ar doped with HC_3N/C_2H_2 mixtures[34] irradiated using a H_2 discharge lamp emitting in the far-UV. It was also seen in Ar, Kr, N_2, and pH_2 solids containing HC_3N alone and photolyzed at 193 nm using a laser.[35] Cyanotriacetylene was detected in solid Ar doped with a mixture of either HC_3N and C_4H_2 (diacetylene) or HC_5N and C_2H_2,[36] and photolyzed either by excimer laser radiation or an H_2 discharge lamp. The HC_7N molecule has also been produced by electric discharges in a mixture of HC_3N and Kr just prior to trapping on a cold window.[37] In all of these cryogenic approaches, the cyanopolyacetylenes generated were found to emit strong phosphorescence which has proved to be the most sensitive spectroscopic indicator of their presence. Here we verified that a mixture of C_4H_2 and HC_5N precursors could couple to produce HC_9N during UV-assisted, low-temperature synthesis. The spectroscopic identification has been supported using density functional theory calculations of electronic and vibrational energy levels.

EXPERIMENT

The precursor molecules were prepared using the methods developed by Trolez & Guillemin[38] (HC_5N) and Khlifi *et al.*[39] (C_4H_2). HC_5N was alternately exposed to vacuum at T<200 K and then warmed to remove CO_2 and other volatile impurities. This cycle was repeated until the rate of pressure rise during warming was negligible. C_4H_2 was subjected to several freeze-pump-thaw cycles (T<200 K, with some loss of the product). Purification of both precursors was carried out directly before the experiments.

Noble gases (Kr 4.0 or Ar 6.0, Messer) were mixed with C_4H_2 and HC_5N at typical ratios of approx. 500:1:1 using standard manometric techniques. This mixture was subsequently trapped on a sapphire substrate window held at either 30 K (Kr) or at 22 K (Ar) as measured and regulated with a Scientific Instruments Inc. 9620-1 temperature controller. The closed-cycle helium refrigerator (Air Products *Displex* DE202FF) was equipped with external CaF_2 windows. The typical amount of deposited gas was 6-8 mmol. Composition of the samples was verified with a Nicolet *Nexus* 670/870 FTIR spectrometer with a maximal resolution of 0.125 cm^{-1} and equipped with a liquid nitrogen-cooled MCT detector. Spectra consisted of 256 or 1024 averaged interferograms. To induce the photochemical transformations of precursor molecules, cryogenic matrices were irradiated with a 193 nm ArF excimer laser (Coherent *Compex Pro*), either during or after the sample deposition. The laser typically operated at a repetition rate of 10 Hz and the energy delivered to the sample surface did not exceed 5 mJ/cm^2 per pulse. While argon is the most commonly used rare gas in matrix experiments, krypton matrices were preferred here, as they have already been shown to supply strong and well resolved spectra of embedded cyanopolyacetylenes.[35,37] Thermal processing, *i.e*. annealing, was accomplished by warming up to ~30-40 K and then re-cooling (only for Kr). The lowest temperature reached for the cryogenic samples was 7 K.

The identification of photolysis products relied on selectively excited electronic luminescence. Two modes of measurement were employed. The first mode involved excitation at a fixed

wavelength followed by recording the resulting dispersed phosphorescence spectrum. This spectrum contains information on vibrational frequencies in the ground electronic state of light emitting products. The second mode gave access to vibrations in an excited singlet state, and relied on scanning the excitation wavelengths while recording the phosphorescence signal. A Continuum Surelite II + OPO Horizon laser system operating in the 192-400 nm range was used for the excitation. The pulse repetition rate of this laser system was 10 Hz. Phosphorescence was dispersed with a 0.6 m Jobin-Yvon grating monochromator and detected with a gated CCD camera (Andor *iStar* DH720) with a detection range of 380-800 nm and a resolution of approx. 0.04 nm. Time synchronization between laser pulses and detection of phosphorescence was provided by a home-made triggering device.

Phosphorescence decay time measurements were performed using a photomultiplier (Hamamatsu H3177-50 PMT) with a detection range of 200 – 850 nm connected to the monochromator. Parallel to the phosphorescence intensity measurements, the excitation laser intensity was monitored with a photodiode.

COMPUTATIONAL DETAILS

All quantum chemical calculations were carried out using density functional theory (DFT).[40] Time-dependent methodologies[41–43] were applied together with the B3PW91 functional of Perdew and Wang[44–47] for all computations of singlet excited electronic states (B3PW91 differs from the better known B3LYP[48] by the non-local correlation term). The B3LYP functional modified with the Coulomb-attenuating method (CAM-B3LYP)[49] was applied in its conventional form to predict the energetic separation between the ground and the lowest triplet state. The Dunning-type basis set aug-cc-pVTZ[50,51] was applied in all computations of this sort and supplied geometries for different electronic states, corresponding harmonic vibrational frequencies, and energies of transitions from the ground to excited electronic states.

To take into account the anharmonicity and inaccuracies of the applied theory, vibrational frequencies were scaled with the factor of 0.96,[52,53] for ground state DFT as well as for excited state TD-DFT computations. For the ground state, IR absorption intensities and Raman activities were also predicted. Linearity of the structure in the excited singlet electronic states was verified by optimizations starting from the bent geometry at the CIS/aug-cc-pVDZ[50,51,54] level and inspection of vibrational frequencies (checking for the degeneracy of bending modes and for the possible occurrence of imaginary frequencies) at both CIS and DFT levels.

Special attention was paid to the formally forbiden $\tilde{B}\ ^1\Delta - \tilde{X}\ ^1\Sigma^+$ system, where vibronic bands could be observed due to Herzberg–Teller coupling with a π-symmetry vibration. In order to identify that promoting mode, we have carried out a series of transition intensity (oscillator strength) calculations for the molecule distorted by each of the bendings. The vector representing the change was always parallel to a given normal coordinate and had a length of 0.1 Å. (Of note, when the movement along a bending normal coordinate of HC_9N is considered, shifts between the equilbrium ground state ($\tilde{X}$, v=0) geometry and any of the two $\tilde{B}$-state vibrational wavefunction $|\Psi_{v=1}|$ maxima are on the order of 0.1 Å.) The Herzberg-Teller effect was assumed to be significant if the coupling to a given π-symmetry vibrational mode, simulated as outlined above, produced the oscillator strength of at least 0.0001.

The GAUSSIAN 09 (Rev. B. 01) program was used for all computations[55] while Jmol,[56] Gabedit,[57] and Chemcraft[58] were used for preparation of inputs and visualization of outputs. Additional computations were performed by DALTON 2.0[59] at the CC2/cc-pVDZ level[60–62] in order to predict the dominant character of the transitions.

RESULTS AND DISCUSSION

Theoretical predictions

Theoretical predictions for the excited electronic states of HC_9N are listed in Table 1. In Figure 1, the corresponding molecular geometries are compared to that of the ground state. The DFT-

derived ground-state structure matches the experimental one reasonably well and suggests that the computational level used is sufficient for this application. The interatomic distances in states $\tilde{A}$, $\tilde{B}$ and $\tilde{a}$, differ by less than 0.7 pm and, compared to $\tilde{X}$, the geometry in these excited states corresponds to an elongation of triple bonds and shortening of the CC single bonds. The electronic structures of $\tilde{A}$, $\tilde{B}$, and $\tilde{a}$, together with that of the $\tilde{E}$ state, come mainly from the HOMO-LUMO excitation. The $\tilde{E}$ state geometry, however, slightly differs from those of the three other HOMO-LUMO states, especially in the middle of the chain, where there is a less pronounced length alternation of consecutive carbon-carbon bonds. The lowest-energy fully allowed electronic excitation is $\tilde{E}\ ^1\Sigma^+ - \tilde{X}\ ^1\Sigma^+$. Orbitally forbidden $\tilde{B}\ ^1\Delta - \tilde{X}\ ^1\Sigma^+$ transitions may however also be quite important (as shown for HC_3N[63–65] and HC_5N[66]), gaining sizable intensity *via* Herzberg–Teller vibronic coupling.

Table 1. Energy (eV) and Oscillator Strength for Transitions Involving the Ground ($X\ ^1\Sigma^+$) and Excited Electronic States of HC_9N Derived at the B3PW91/aug-cc-pVTZ Level of Theory. Wavelengths (nm) Corresponding to the Transitions are Given in Parentheses.

State [a]	Dominant orbital excitation	Vertical transition energy (λ)	f [b]	*0-0* transition energy (λ)
$\tilde{A}\ ^1\Sigma^-$	$5\pi\rightarrow1\pi^*$	2.84 (437)	0	2.39 (519)
$\tilde{B}\ ^1\Delta$	$5\pi\rightarrow1\pi^*$	2.93 (423)	0	2.52 (492)
$\tilde{C}\ ^1\Sigma^-$	$4\pi\rightarrow1\pi^*$	4.38 (283)	0	4.10 (302)
$\tilde{D}\ ^1\Delta$	$4\pi\rightarrow1\pi^*$	4.53 (274)	0	4.27 (290)
$\tilde{E}\ ^1\Sigma^+$	$5\pi\rightarrow1\pi^*$	5.06 (245)	2.8	4.88 (254)
$\tilde{F}\ ^1\Sigma^-$	$5\pi\rightarrow2\pi^*$	5.30 (234)	0	4.98 (249)
$\tilde{G}\ ^1\Delta$	$5\pi\rightarrow2\pi^*$	5.32 (233)	0	5.00 (248)
$\tilde{H}\ ^1\Sigma^+$	$4\pi\rightarrow1\pi^*$, $5\pi\rightarrow2\pi^*$	5.40 (230)	1.7	5.11 (243)
$\tilde{a}\ ^3\Sigma^+$	$5\pi\rightarrow1\pi^*$	-	-	2.16 (574)

[a] Ground state electronic configuration: [core] $(1\sigma)^2\ (2\sigma)^2\ (3\sigma)^2\ (4\sigma)^2\ (5\sigma)^2\ (6\sigma)^2\ (7\sigma)^2\ (8\sigma)^2\ (9\sigma)^2\ (10\sigma)^2\ (1\pi)^4\ (2\pi)^4\ (11\sigma)^2\ (3\pi)^4\ (4\pi)^4\ (5\pi)^4\ (1\pi^*)^0\ (2\pi^*)^0\ (1\sigma^*)^0$.

[b] Value of zero indicates $f < 5 \cdot 10^{-5}$.

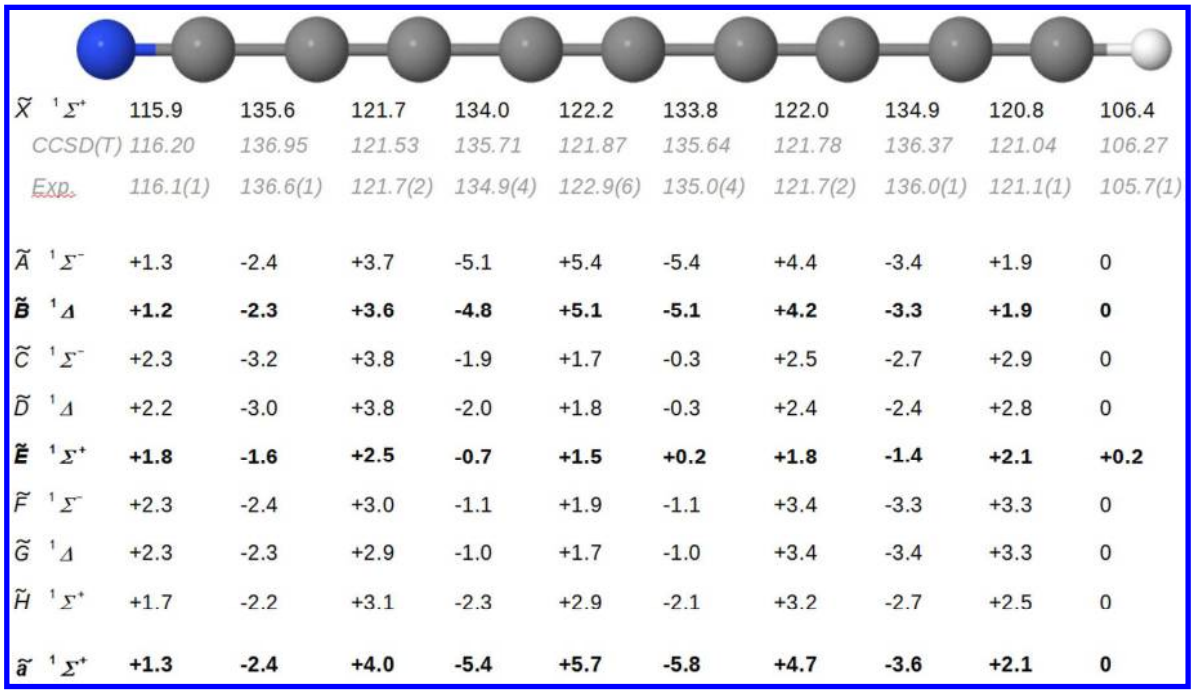

$\tilde{X}$ $^1\Sigma^+$	115.9	135.6	121.7	134.0	122.2	133.8	122.0	134.9	120.8	106.4
CCSD(T)	*116.20*	*136.95*	*121.53*	*135.71*	*121.87*	*135.64*	*121.78*	*136.37*	*121.04*	*106.27*
Exp.	*116.1(1)*	*136.6(1)*	*121.7(2)*	*134.9(4)*	*122.9(6)*	*135.0(4)*	*121.7(2)*	*136.0(1)*	*121.1(1)*	*105.7(1)*
$\tilde{A}$ $^1\Sigma^-$	+1.3	-2.4	+3.7	-5.1	+5.4	-5.4	+4.4	-3.4	+1.9	0
$\tilde{B}$ $^1\Delta$	**+1.2**	**-2.3**	**+3.6**	**-4.8**	**+5.1**	**-5.1**	**+4.2**	**-3.3**	**+1.9**	**0**
$\tilde{C}$ $^1\Sigma^-$	+2.3	-3.2	+3.8	-1.9	+1.7	-0.3	+2.5	-2.7	+2.9	0
$\tilde{D}$ $^1\Delta$	+2.2	-3.0	+3.8	-2.0	+1.8	-0.3	+2.4	-2.4	+2.8	0
$\tilde{E}$ $^1\Sigma^+$	**+1.8**	**-1.6**	**+2.5**	**-0.7**	**+1.5**	**+0.2**	**+1.8**	**-1.4**	**+2.1**	**+0.2**
$\tilde{F}$ $^1\Sigma^-$	+2.3	-2.4	+3.0	-1.1	+1.9	-1.1	+3.4	-3.3	+3.3	0
$\tilde{G}$ $^1\Delta$	+2.3	-2.3	+2.9	-1.0	+1.7	-1.0	+3.4	-3.4	+3.3	0
$\tilde{H}$ $^1\Sigma^+$	+1.7	-2.2	+3.1	-2.3	+2.9	-2.1	+3.2	-2.7	+2.5	0
$\tilde{a}$ $^1\Sigma^+$	**+1.3**	**-2.4**	**+4.0**	**-5.4**	**+5.7**	**-5.8**	**+4.7**	**-3.6**	**+2.1**	**0**

Figure 1. HC_9N geometry in its ground and excited electronic states as derived at the B3PW91/aug-cc-pVTZ level of theory. Interatomic distances in pm. Values listed for the excited electronic states are relative, calculated with respect to $\tilde{X}$. Also given are the ground-state experimental distances[20] together with their respective CCSD(T) predictions[19]. The states $\tilde{a}$, $\tilde{B}$, and $\tilde{E}$ were experimentally observed in this work (entries listed in bold).

Vibrational frequencies characterizing $\tilde{X}$, $\tilde{B}$, and $\tilde{E}$ states are listed in Table 2, together with $\tilde{X}$-state IR absorption intensities and Raman scattering activities. Predictions obtained for the remaining singlet excited states of Tab. 1 and Fig. 1 can be found in Tab. S1 of the Supporting Information. Table 2 provides also a short description of vibrational modes (see Tab. S2 of the Supporting Information for the graphical representations). The corresponding modes closely resemble one another in these three electronic states with the exception of modes in the 2000-2200 cm^{-1} range where the vibrations represent diverse mixtures of C≡C and C≡N stretches.

Table 2. Harmonic Vibrational Frequencies (in cm^{-1}; Scaling Factor 0.96) for the Ground and Two Excited Electronic States of HC_9N, as Derived at the B3PW91/aug-cc-pVTZ Level of Theory. IR Intensity and Raman Activity Units are km/mol and $Å^4$/amu, Respectively.

Mode	$\tilde{X}$		$\tilde{B}$	$\tilde{E}$	Short description [a]
	Freq.	IR intensity/ *Raman activity*	Freq.	Freq.	
	σ symmetry				
ν_1	3324	193/*12*	3318	3298	νCH
ν_2	2250	109/*1922*	2098	2150	Mixture of νC≡C and νC≡N
ν_3	2201	1.5/*473*	2059	2059	Mixture of νC≡C and νC≡N
ν_4	2146	291/*32763*	2000	2033	Mixture of νC≡C and νC≡N
ν_5	2122	8.2/*3523*	1900	1956	Mixture of νC≡C and νC≡N
ν_6	2037	0.1/*1511*	1848	1893	Mixture of νC≡C and νC≡N
ν_7	1369	0.5/*0.3*	1479	1346	Adjacent νC-C out of phase
ν_8	1074	0.5/*38*	1106	1071	νC-CH + νC-CN in phase
ν_9	736	3.9/*1.5*	741	730	νC-CH + νC-CN out of phase
ν_{10}	376	0.3/*1.6*	386	374	Chain stretch
	π symmetry				
ν_{11}	764	0.1/*39*	754	712	Chain bending (*zig-zag*; 9 nodes)
ν_{12}	640	40/*13*	559	562	δCH
ν_{13}	578	0.5/*0.0*	547	519	Chain bending (8 nodes)
ν_{14}	511	4.2/*12*	486	458	Chain bending (7 nodes)
ν_{15}	451	0.1/*0.9*	432	419	Chain bending (6 nodes)
ν_{16}	301	4.0/*0.0*	309	253	Chain bending (5 nodes)
ν_{17}	198	0.1/*1.1*	191	147	Chain bending (4 nodes)
ν_{18}	107	4.4/*1.2*	105	88	Chain bending (3 nodes)
ν_{19}	40	0.1/*0.9*	39	35	Chain bending (2 nodes)

[a] ν - stretching; δ - bending.

Detection of HC_9N

Since both C_4H_2 and HC_5N precursors are strong phosphorescence emitters[66,67] with long vibronic progressions in the UV-visible range, it was important to have reliable predictions concerning the electronic spectroscopy of HC_9N, in order to unambiguously distinguish the product from its precursors.

In the homologous series of polyynes, UV absorption wavelengths have been shown to change almost linearly with the size of the chain.[68,69] This can be simplistically rationalized by considering a classical particle-in-a-box model, where a valence electron (a 'particle') is delocalized in a system ('box') of conjugated bonds.[68] Prior to the present study, phosphorescence of HC_7N,[36] HC_5N,[35] and C_3N^- anion[70] has been observed (HC_3N, isoelectronic with C_3N^-, does not phosphoresce), and the wavelengths of the corresponding vibrationless $\tilde{a} - \tilde{X}$ emission origins were found to be linearly correlated with the length of the carbon-nitrogen chain.[36] Extrapolation of this empirical trend places the origin of HC_9N phosphorescence near 588 nm or 2.11 eV. CAM-B3LYP calculations (Table 1) predict a value of 574 nm or 2.16 eV (Figure 2).

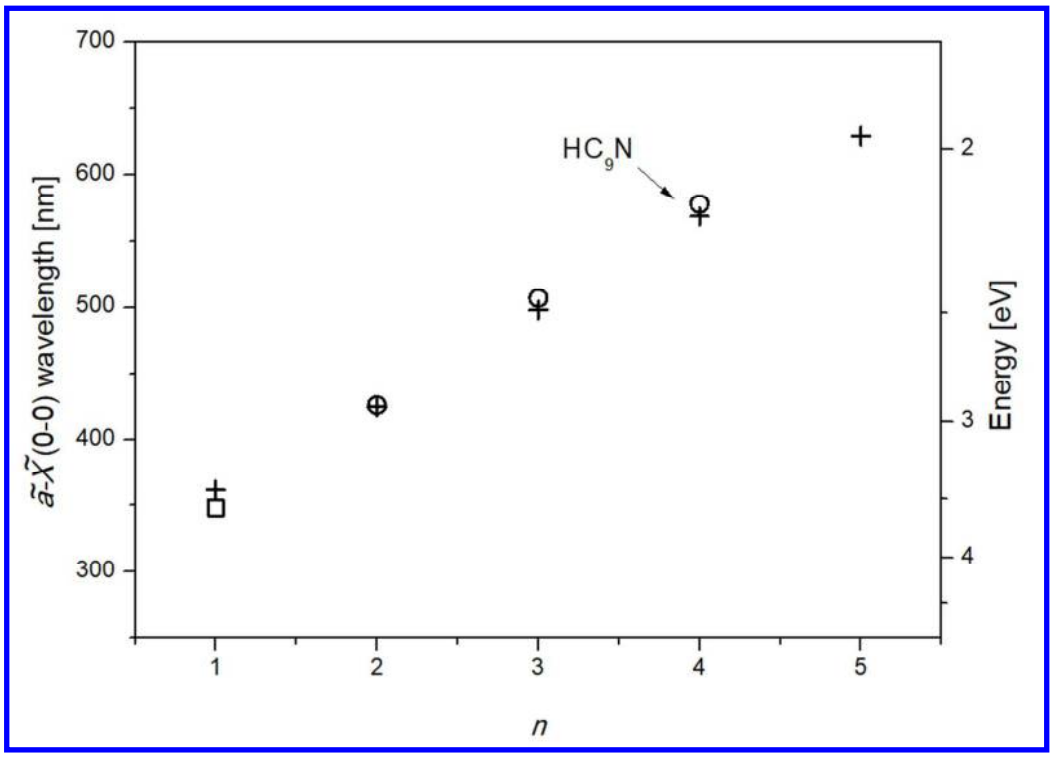

Figure 2. Phosphorescence origin wavelength as a function of carbon chain length for $HC_{2n+1}N$ molecules. Circles mark the experimental values for Kr matrices (HC_3N does not phosphoresce; value observed for the isoelectronic C_3N^- anion[70] is entered for n=1 as an open square). Crosses correspond to CAM-B3LYP/aug-cc-pVTZ predictions. Experimental data for HC_5N and HC_7N come from Refs. 37,66.

While our CCD camera and spectrograph were well suited to record the anticipated HC_9N phosphorescence, we did not rely on exciting this emission with the ArF excimer laser (193 nm) employed for the photolysis. Instead, selective excitation of a sample previously subjected to extensive 193 nm irradiation was performed using a less powerful, tunable OPO operating in the expected region of $\tilde{E} - \tilde{X}$ transitions (around 250 nm). The corresponding dispersed phosphorescence spectra showed a 578 nm band which was the origin of a vibronic progression and whose excitation spectrum exhibited strong bands between 240 and 260 nm (as shown later). Once the emission and excitation wavelengths of HC_9N phosphorescence were determined, it was possible to follow the photochemical reaction kinetics in a fresh $Kr/C_4H_2/HC_5N$ sample. For these measurements, the intensity of the 578 nm emission induced *via* OPO excitation (273.7 nm) was monitored over the course of 193 nm excimer laser irradiation. Time delays on the

order of a few to tens of ms between the OPO, excimer laser, and signal acquisition were fixed to avoid, as much as possible, any perturbation of the collected spectrum by the phosphorescence of precursors excited at 193 nm. The time evolution of the resulting signal is depicted in Figure 3. No signal could be seen for an unphotolyzed sample showing that the emission certainly came from a photoproduct. The growth rate of this species decreased with irradiation time.

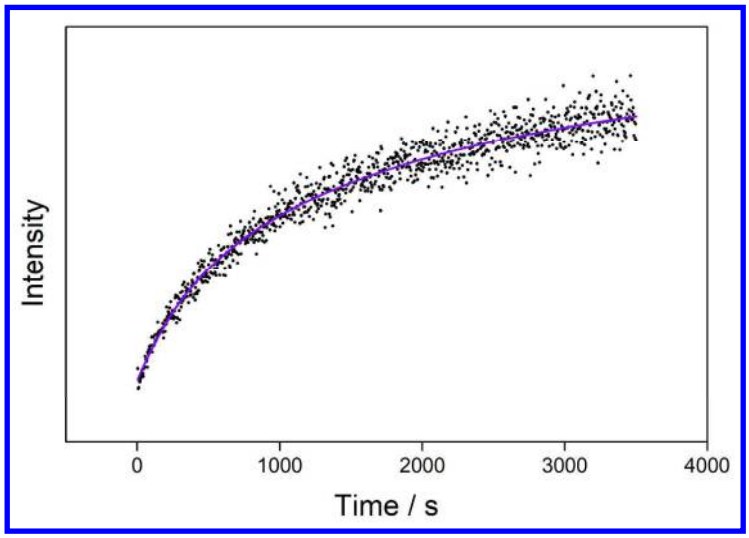

Figure 3. Time evolution of HC_9N formation, as monitored by intensity of phosphorescence (excited at 273.7 nm and measured at 578 nm) emitted from an irradiated (193 nm) $Kr/C_4H_2/HC_5N$ (1000/1/1) matrix. Solid line added for better visibility of the trend.

Phosphorescence and vibrational modes of the ground state

The luminescence presented in Figure 4 was emitted from UV-photolyzed $Kr/C_4H_2/HC_5N$ matrices. The first intense band at 17 300 cm^{-1} (578 nm, 2.14 eV) is the origin of the $\tilde{a} - \tilde{X}$ transition of HC_9N and almost matches the theoretical prediction. This band is clearly correlated to those around 15 150 and 13 000 cm^{-1}; all three groups of spectral features share a common phosphorescence excitation spectrum. Two vibronic bands, separated from the *0-0* transition by 2143 cm^{-1} and 2170 cm^{-1}, can be distinguished in the spectrum and are indicative of excitation of triple bond stretching vibrations. The former can be assigned to mode ν_4 of HC_9N (*cf.* predicted $\tilde{X}$-state frequencies listed in Table 2). This mode corresponds to the in-phase stretching of the

three central C≡C bonds (see Table S2). Mode ν_4 is likely to play the key role in phosphorescence transitions, as it deforms the molecule (alternately shrinking and elongating the consecutive bonds along the chain) in a similar fashion as predicted for electronic transitions between states $\tilde{X}$ and $\tilde{a}$ (Fig. 1). Stretching modes having similar characteristics also shaped the main vibronic progressions in low-temperature phosphorescence of HC_5N,[35,66] and HC_7N.[36,37] These modes also had the highest Raman activity in ground electronic states of the said cyanopolyynes. This is also true for the Raman activity of ν_4 in the ground electronic state of HC_9N (Table 2). The spacing of 2170 cm^{-1} is unlikely to be associated with ν_3. There is a poor match with the predicted ν_3 value of 2201 cm^{-1} and atomic displacements involved in the vibration (Table 2 and Table S2) are qualitatively different from those of ν_4. We propose assignment of this spacing to $2\nu_8$ (harmonic prediction: $2 \cdot 1074$ cm^{-1}). Mode ν_8 is C-C stretching, resembling *gerade* symmetry. A similar vibronic spacing, produced by a C-C stretching overtone ($2\nu_5$), was observed for HC_5N.[66] Assignments of several vibronic bands of HC_9N in Kr and in Ar hosts are proposed in Table 3. A π-symmetry mode, possibly ν_{14}, was observed only in Ar (497 cm^{-1} with respect to the vibrationless origin); an alike bending-mode vibronic band of HC_5N phosphorescence was intense in Ar and weak in Kr.[66]

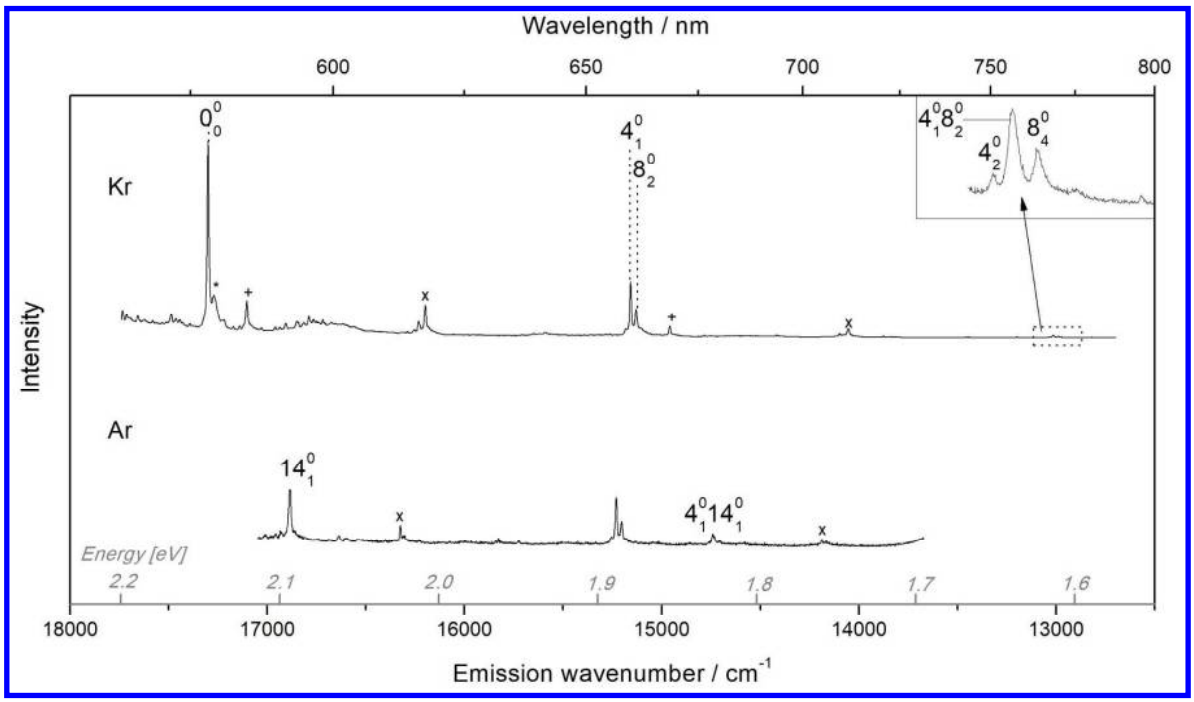

Figure 4. HC_9N-dominated phosphorescence of photolyzed (193 nm) $Kr/C_4H_2/HC_5N$ (1000/1/1) (upper) and $Ar/C_4H_2/HC_5N$ (1000/1/1) (lower) matrices excited at 36 540 cm^{-1} (273.7 nm) and 41 440 cm^{-1} (241.3 nm), respectively. Bands marked with '+' belong to additional photolysis products (as determined with the analysis of phosphorescence excitation spectra). The asterisked band is interpreted as being due to a secondary matrix site. Bands marked with 'x' are assigned to $C_{10}N_2$ phosphorescence (to be reported separately).

Table 3. Wavenumbers (in cm^{-1}) of Electronic Emission Bands Assigned to HC_9N Phosphorescence in Solid Ar and Kr.

Ar		Kr		Assignment
Absolute	Relative[a]	Absolute	Relative[a]	
17379	0	17300	0	0_0^0
16881	497			14_1^0
15231	2148	15157	2143	4_1^0
15205	2174	15130	2170	8_2^0
14740	2639			$4_1^0 14_1^0$
		13038	4262	4_2^0
		13018	4282	$4_1^0 8_2^0$

		12992	4308	8_4^0

[a] Relative values give distances from the vibrationless origin.

No IR absorption attributable to HC_9N could be measured. This is not surprising, considering that earlier, analogous experiments aimed at synthesizing longer chains from $HC_3N + C_2H_2$ or from $HC_5N + C_2H_2$ led to fairly weak IR bands for HC_5N,[34] and bands near the limit of HC_7N detection,[36] respectively. Furthermore, the yield of (poly)acetylene+cyano(poly)acetylene reactions in rigid matrices is likely decreasing with the increasing size of a cyanopolyacetylenic product.

The phosphorescence decay time in solid krypton, 3.9 ± 0.1 ms (*0-0* band), was for HC_9N smaller than for other members of the $HC_{2n+1}N$ homologous series including HC_5N (40 ms)[66] and HC_7N (8.2 ms)[71]. The increased number of internal degrees of freedom presumably promotes non-radiative relaxation channels, decreasing the triplet state lifetime. As chains get longer, the phosphorescence lifetime can be expected to decrease further.

Singlet excited electronic states

The excitation spectrum of HC_9N phosphorescence revealed two distinct electronic systems, in 26 000 – 34 000 cm^{-1} and 35 000 – 50 000 cm^{-1} regions.

The first (Figure 5), characterized by a series of bands spaced by ~2100 cm^{-1}, was assigned to $\tilde{B}\ ^1\Delta - \tilde{X}\ ^1\Sigma^+$ transitions, based on very similar patterns already observed in UV absorption and/or phosphorescence excitation spectra for the smaller molecules of the series: HC_3N,[63–65] HC_5N,[66] and HC_7N.[72] Geometry changes implied by $\tilde{B} - \tilde{X}$ and $\tilde{a} - \tilde{X}$ excitations are mutually similar (see Figure 1), therefore both systems are expected to feature alike vibronic patterns. One of possible choices for the mode responsible for the vibronic $\tilde{B} - \tilde{X}$ progression is ν_3, because the corresponding vibrational motions of atoms in the $\tilde{B}$ state (see Table S2 for visualization) resemble those of ν_4 in the ground electronic state (ν_4 already mentioned as prominently appearing in $\tilde{a}$-$\tilde{X}$ phosphorescence). While we cannot exclude the above possibility, we prefer to

assign the $\tilde{B} - \tilde{X}$ progression to the stretching mode ν_2, for which the predicted $\tilde{B}$-state frequency better matches the observed vibronic spacing (see Table 2).

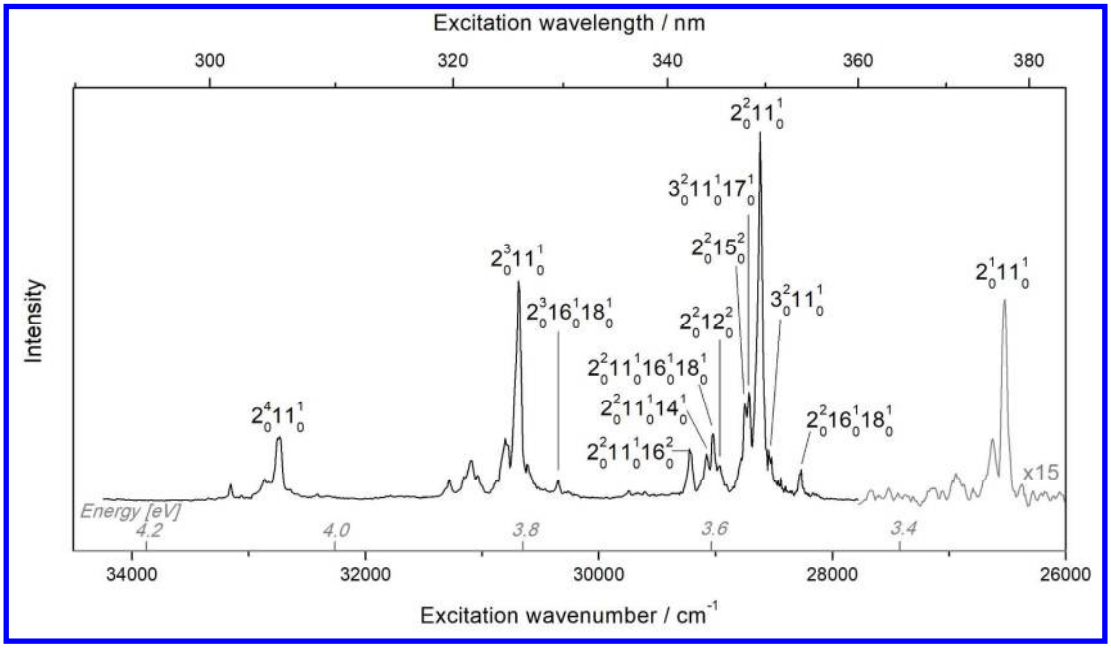

Figure 5. $\tilde{B}\ ^1\Delta - \tilde{X}\ ^1\Sigma^+$ system detected in the phosphorescence excitation spectrum of HC_9N, coming from a previously photolyzed (193 nm) $Kr/C_4H_2/HC_5N$ (1000/1/1) matrix. Detection centered at the most intense phosphorescence band (17 300 cm^{-1}, 2.14 eV). Wavelength-dependent laser intensity variations might distort the phosphorescence intensity pattern.

No band corresponding to the $\tilde{B} - \tilde{X}$ origin is expected to appear in the spectrum, since the transitions of this orbital symmetry-forbidden system require coupling to a π-symmetry vibrational mode. In the analysis of respective analogous $\tilde{B} - \tilde{X}$ transitions, such π-symmetry modes were identified as ν_5 for HC_3N,[63–65] ν_8 for HC_5N,[66] and ν_{10} and/or ν_{12} for HC_7N.[72] Looking at the common features of the above vibrations, one can find that: (*i*) these are the chain bendings of the highest energy, sharing specific, qualitatively similar molecular distortion patterns, and (*ii*) their ground and excited state frequencies are very different. Moreover, in the case of Ar matrix-isolated HC_5N, the ν_8 mode stands out in the phosphorescence spectrum.[66] For HC_9N, it was in principle possible to assign the observed vibronic features assuming the participation of either ν_{11}, ν_{12}, or ν_{14} (predicted $\tilde{B}$-state wavenumbers: 754 cm^{-1}, 559 cm^{-1} and

486 cm^{-1}, respectively). To further narrow down which of the three modes is involved, $\tilde{B} - \tilde{X}$ oscillator strength values were derived for $\tilde{B}$-state molecular geometry slightly distorted along respective normal bending coordinates (see Computational Details). A noticeable oscillator strength has appeared only for the geometry distorted along the coordinate of mode ν_{11}. This coarse computational simulation of the Herzberg-Teller coupling suggests that the $\tilde{B} \leftarrow \tilde{X}$ absorption may gain probability *via* excitation of the ν_{11} mode in the upper electronic state. The corresponding assignment is given in Figure 5 and Table 4 using the theoretical values of Table 2 for vibrational frequencies. Assuming that ν_{11} is the promoting mode, the origin of $\tilde{B} - \tilde{X}$ can be expected approximately 750 cm^{-1} below the first detectable band of the ν_2 progression (26 530 cm^{-1}), namely at ~25 780 cm^{-1} (388 nm). However, DFT calculations (Table 1) locate the vibrationless $\tilde{B} - \tilde{X}$ origin much lower, at 492 nm (20 330 cm^{-1}). As taken into account in Figure 5 and Table 4, this implies the presence of at least one additional, less energetic element of the ν_2 progression and a possible placement of the system origin around 23 700 cm^{-1} (corresponding to 422 nm, which is out of the detection range limited here to $\lambda < 400$ nm).

Table 4. Vibronic Bands in the $\tilde{B}\ ^1\Delta - \tilde{X}\ ^1\Sigma^+$ Electronic System of HC_9N in Solid Krypton, Revealed by the Phosphorescence Excitation Spectrum.

Frequency (cm^{-1})		Assignment
Absolute	Relative[a]	
26533	**0**	$\mathbf{2_0^1 11_0^1}$
26925	392	$2_0^1 11_0^1 16_0^1 18_0^1$
27150	617	$2_0^1 11_0^1 16_0^2$
28165	1632	$2_0^2 17_0^1 18_0^1$
28274	1741	$2_0^2 16_0^1 18_0^1$
28546	2013	$3_0^2 11_0^1$ / $2_0^2 14_0^1 17_0^1$
28623	**2090**	$\mathbf{2_0^2 11_0^1}$
28719	96	$3_0^2 11_0^1 17_0^1$ / $2_0^2 11_0^1 18_0^1$

28753	130	$2_0^2 15_0^2$
28970	347	$2_0^2 12_0^2$
29027	404	$2_0^2 11_0^1 16_0^1 18_0^1$
29083	460	$2_0^2 11_0^1 14_0^1$
29225	602	$2_0^2 11_0^1 16_0^2$
29606	983	$2_0^2 11_0^1 12_0^1 15_0^1$
29743	1120	$2_0^2 11_0^1 12_0^2$
30267	1644	$2_0^3 17_0^1 18_0^1$
30349	1726	$2_0^3 16_0^1 18_0^1$
30613	1990	$3_0^3 11_0^1$ /$2_0^3 14_0^1 17_0^1$
30691	**2068**	$\mathbf{2_0^3 11_0^1}$
30780	89	$3_0^3 11_0^1 17_0^1$ / $2_0^3 11_0^1 18_0^1$
30807	116	$2_0^3 15_0^2$
31040	349	$2_0^3 12_0^2$
31098	407	$2_0^3 11_0^1 16_0^1 18_0^1$
31155	464	$2_0^3 11_0^1 14_0^1$
31281	590	$2_0^3 11_0^1 16_0^2$
32324	1633	$2_0^4 17_0^1 18_0^1$
32408	1717	$2_0^4 16_0^1 18_0^1$
32639	1948	$3_0^4 11_0^1$ / $2_0^4 14_0^1 17_0^1$
32734	**2043**	$\mathbf{2_0^4 11_0^1}$
32828	94	$3_0^4 11_0^1 17_0^1$ / $2_0^4 11_0^1 18_0^1$
32862	128	$2_0^4 15_0^2$
33152	418	$2_0^4 11_0^1 16_0^1 18_0^1$

[a] Relative values give distances from the previous member of the $2_0^n 11_0^1$ progression (bold).

The systematic bathochromic shift of $\tilde{B} - \tilde{X}$ spectra with increasing the $HC_{2n+1}N$ chain length is shown in Figure 6. While singlet-triplet energy splittings are well predicted by DFT (Figure 2), $\tilde{B} - \tilde{X}$ excitation energies are sizably underestimated (note that the ordinate axis in Figure 6 corresponds to wavelength). It is still true after accounting for a gas-to-matrix shift on the order

of 5 nm. Accidentally, our DFT-derived *vertical* transition energies match the experimental $\tilde{B} - \tilde{X}$ origin values. As exemplified e.g. by a recent study[73] for atoms, TD-B3PW91/aug-cc-pVTZ excitation energies tend, on average, to be underestimated by a few percent. For the series of molecules investigated here, this TD-DFT error happens to have a similar size as the difference between vertical and vibrationless transitions. The plot adds credibility to the analysis of the HC_9N phosphorescence excitation spectrum presented above, and in particular to the ensuing derivation of the $\tilde{B} - \tilde{X}$ origin (at ~422 nm, represented by a black dot for n=4). Indeed, had our assignment of $2_0^1 11_0^1$ been incorrect, the first band of the progression would have had to be assigned to $2_0^2 11_0^1$, placing the system origin at ~465 nm. The red dot, depicting that latter possibility in Figure 6, spoils a trend set by lower n values.

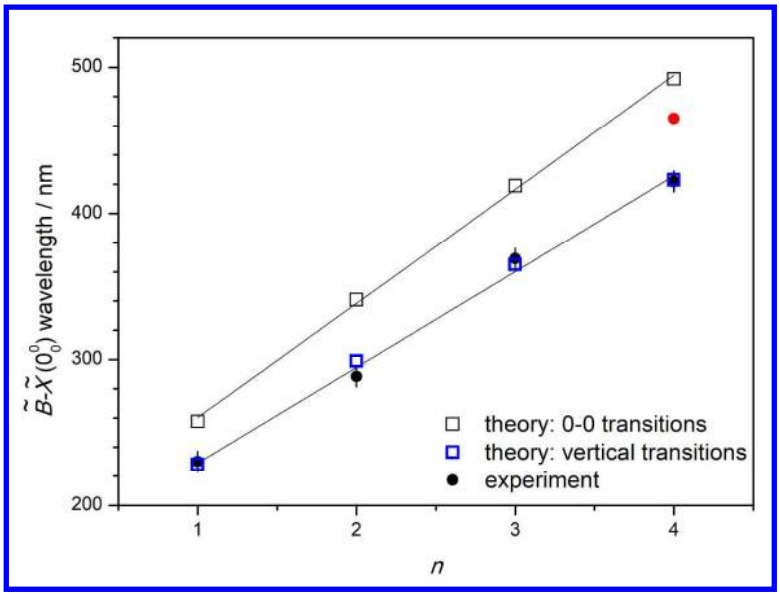

Figure 6. Dependence of the $\tilde{B}$-$\tilde{X}$ system origin wavelength on the carbon chain size (n), for $HC_{2n+1}N$ molecules. Data based on Kr-matrix measurements, with the exception of n = 1 measured in solid Ar (expected Kr-to-Ar wavelength shift is on the order of 0.5 nm). Theoretical predictions carried out at the TD-B3PW91/aug-cc-pVTZ level of theory. Red dot assumes misassignment of the first element of the progression (see text).

The second series consists of intense bands in the 35 000 – 50 000 cm^{-1} range of the HC_9N phosphorescence excitation spectrum and coincides with the spectral region of fully allowed $\tilde{E}$

$^1\Sigma^+ - \tilde{X}\ ^1\Sigma^+$ and $\tilde{H}\ ^1\Sigma^+ - \tilde{X}\ ^1\Sigma^+$ systems. These features can be compared (see Figure 7) to those of HC_9N observed in UV absorption spectra following the laser ablation of graphite in acetonitrile[31] or to the ones found in a similar, though less detailed, UV absorption spectrum (not presented here) of a solution produced after immersion of a carbon arc in liquid ammonia.[30] The DFT-computed $\tilde{E} - \tilde{X}$ vertical excitation energy of 5.06 eV (40 820 cm^{-1}) reasonably corresponds to the maximal signal in Figure 7. The theoretically predicted vertical transitions of several electronic systems marked in Figure 7 point to a high density of states in the spectral window. This impedes reliable identification of individual bands. The complexity of the spectrum is presumably due to a mixing of vibronic transitions involving various electronic states. The lowest-energy band in this region, at 34 600 cm^{-1} (4.29 eV), is weak and strongly red-shifted with respect to the predicted $\tilde{E} - \tilde{X}$ origin (4.88 eV). Noteworthy, a substantial *blue* shift was observed between experimental and theoretical $\tilde{B} - \tilde{X}$ transitions (Figure 5). The 34 600 cm^{-1} band may therefore belong to the $\tilde{D}\ ^1\Delta - \tilde{X}\ ^1\Sigma^+$ system, similar in nature to $\tilde{B}\ ^1\Delta - \tilde{X}\ ^1\Sigma^+$ transitions, partly allowed owing to Herzberg–Teller vibronic coupling. Band progressions starting at 34 600 cm^{-1} can be followed up to around 42 000 cm^{-1}. The vibronic spacings of approx. 1950 cm^{-1} could correspond to $\tilde{D}$-state C≡C stretchings. Two examples of such progressions are marked in Figure 7 (lower energy part). A very narrow band observed at 39 610 cm^{-1} (4.91 eV) is possibly the origin of $\tilde{E}\ ^1\Sigma^+ - \tilde{X}\ ^1\Sigma^+$ system (which would make a good agreement with the theoretical prediction of Table 1). There are no evident candidates for other $\tilde{E} - \tilde{X}$ transitions. However, the pattern of intense bands in Figure 7 resembles the one obtained in the excitation spectrum of HC_7N [37] around the first fully allowed electronic transition. Figure S1 of the Supporting Information provides a direct comparison of HC_7N and HC_9N observed in our experiments. It suggests that other bands of $\tilde{E} - \tilde{X}$ are present in this spectrum, contributing to the most intense features. Apart from the excitations to $\tilde{D}$ and $\tilde{E}$, the states $\tilde{G}$ or $\tilde{H}$ may also be considered. The proposed assignment of progressions in Figure 7 points to 41 970 cm^{-1} (5.20 eV) as the origin of the allowed $\tilde{H}\ ^1\Sigma^+ - \tilde{X}\ ^1\Sigma^+$ system (implying a

slight blue shift from the theoretical value of Table 1). Just as in the case of $\tilde{D} - \tilde{X}$ or $\tilde{B} - \tilde{X}$, the vibronic progressions of $\tilde{G} - \tilde{X}$ and $\tilde{H} - \tilde{X}$ should involve a specific triple bond stretching mode of the upper electronic state. A very tentative interpretation of the main bands discussed here is presented in Table 5.

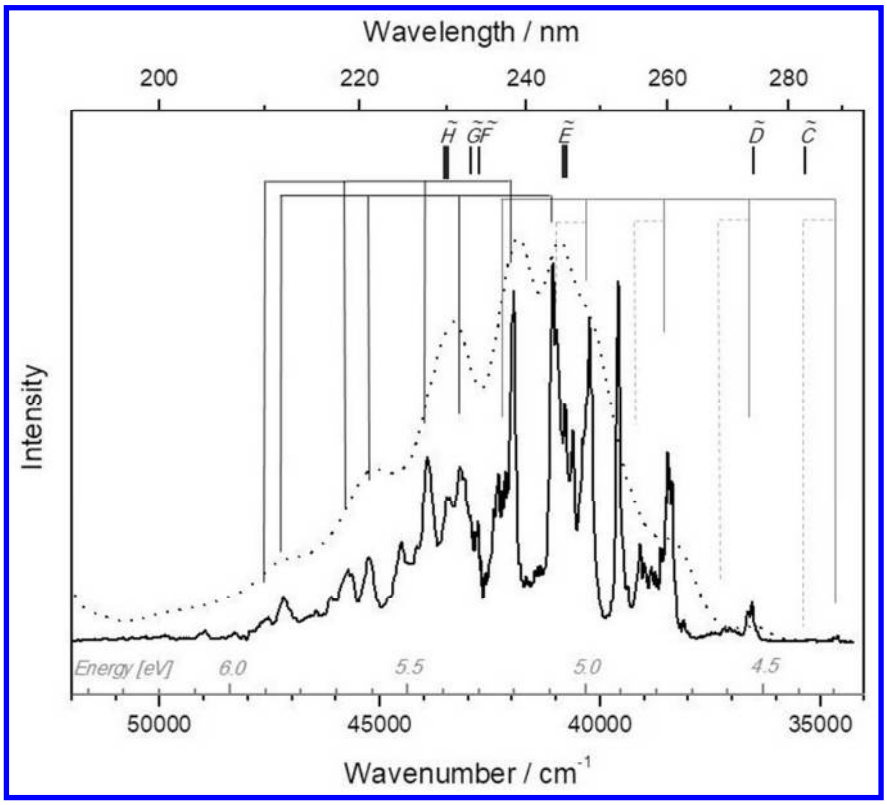

Figure 7. A fragment of the HC_9N phosphorescence excitation spectrum (detection centered at 17 300 cm^{-1}), measured for a previously photolyzed (193 nm) $Kr/C_4H_2/HC_5N$ (1000/1/1) sample, compared to the room-temperature absorption spectrum of HC_9N in acetonitrile (dotted; Wakabayashi *et al.*[31]). Wavelength-dependent laser intensity variations might distort the phosphorescence intensity pattern. Theoretically predicted energies of $\tilde{X}$-originating vertical electronic excitations (data of Table 1) are indicated by top bars (bold ones for the fully allowed transitions). Also marked are the tentatively discerned vibronic progressions (see Table 5).

Couplings between nearly isoenergetic vibronic levels of adjacent electronic states can occur. These may have a sensitive dependence on the chemical environment. Interaction with solvent can lead to the broadening of spectral lines as can differences in temperature at which the spectrum was taken. Although not pictured here, the excitation spectrum of HC_9N in solid Ar

exhibited, when compared to that registered for solid Kr, non-uniform, matrix-related spectral shifts, as might be expected for a mixture of bands originating in various electronic systems. Low S/N ratio in measurement of the Ar matrices did not allow for any vibronic patterns to be reliably discerned. Further studies in varied cryogenic matrices will help in proposing further spectral assignments and in verifying those of Table 5.

Table 5. Vibronic Bands Tentatively Attributed to Excited Singlet States in the HC_9N Phosphorescence Excitation Spectrum of Figure 7.

$\tilde{\nu}$ (cm^{-1})	Provisional assignment
34 598	$\widetilde{D}$ (main progression)
34 706	$\widetilde{D}$
35 288	$\widetilde{D}$ (secondary progression)
36 554	$\widetilde{D}$ (main progression)
36 647	$\widetilde{D}$
37 201	$\widetilde{D}$ (secondary progression)
38 358	$\widetilde{D}$ (main progression)
38 449	$\widetilde{D}$
39 085	$\widetilde{D}$ (secondary progression)
39 605	$\tilde{E}$
40 252	$\widetilde{D}$ (main progression)
40 986	$\widetilde{D}$ (secondary progression)
41 070	$\tilde{G}$ / $\tilde{E}$
41 973	$\widetilde{H}$ / $\tilde{E}$
42 148	$\widetilde{D}$ (main progression)
43 189	$\tilde{G}$
43 921	$\widetilde{H}$
45 247	$\tilde{G}$
45 729	$\widetilde{H}$
47 201	$\tilde{G}$

47 534	$\tilde{H}$

Chain growth mechanism

For a bimolecular photochemical reaction between C_4H_2 and HC_5N (or between any other closed-shell precursors) to occur in a cryogenic matrix, at least one of these molecules must first undergo dissociation or electronic excitation. Following such an event, the excited molecule(s) or radical(s) may come into contact with a reaction partner. As mobility of large molecules is greatly hindered in cryogenic matrices, the reactants should be in the same or adjacent matrix sites for the process to proceed with any probability. Having reactants in the same matrix site may imply the existence of an intermolecular complex prior to excitation/dissociation. If reaction partners are in neighboring sites, some small fraction may already be appropriately oriented for reaction while others must undergo reorientation such that appropriate contact with a partner can be made. Reorientation energy may come from exothermicity of the preceding reactions or from local heating supplied by the photolysing radiation. This leaves a number of possible reaction mechanisms to be explored, some of which can be ruled out.

Dissociation of the cyanide containing species was previously suggested as being responsible for the formation of HC_7N in cryogenic matrices[36] (reactions 1-3). This mechanism is consistent with that proposed by Cherchneff *et al.* for the formation of long chains in the ISM.[16,17]

$$HC_{2n+1}N + h\nu \rightarrow H^{\bullet} + C_{2n+1}N^{\bullet}, \quad (1)$$

$$C_3N^{\bullet} + HC_4H \rightarrow HC_7N + H^{\bullet}, \quad (2)$$

$$C_5N^{\bullet} + HC_2H \rightarrow HC_7N + H^{\bullet}. \quad (3)$$

Dissociation of acetylene or diacetylene to form $C_2H^{\bullet}$ or $C_4H^{\bullet}$ radicals was deemed less significant on the basis of the higher acidity of HC_5N or cyanide containing polyynes in general. Abstraction of the acetylene proton by the cyanide containing radical was ruled out on the basis

of isotopic substitution experiments, although this process would not lead to formation of a longer chain.[36]

It is reasonable to expect that formation of HC_9N proceeds in a similar fashion starting with (1) and followed by (4) below:

$$C_5N^{\bullet} + HC_4H \rightarrow HC_9N + H^{\bullet}. \quad (4)$$

The same products may arise following the formation of $^{\bullet}C_4H$:

$$HC_5N + {}^{\bullet}C_4H \rightarrow HC_9N + H^{\bullet}. \quad (5)$$

Each of these mechanisms entails the absorption of a single photon by a C_4H_2/HC_5N pair. The two precursors should be in close contact or, possibly, occupy neighboring matrix cages.

Just to be complete, one should also consider several other possibilities. The first is a mechanism involving the recombination of radicals:

$$HC_4^{\bullet} + C_5N^{\bullet} \rightarrow HC_9N. \quad (6)$$

Another might be reactions within existing intermolecular complexes where the reactants are hydrogen bonded in a linear arrangement. Such complexes have been used to explain formation of HC_5N from matrix-isolated cyanoacetylene:[35]

$$HC_3N\cdots HC_3N + h\nu \rightarrow HC_5N + CN^{\bullet} + H^{\bullet} \quad (7)$$

A scheme similar to (7) involving the intermolecular complex $HC_3N\cdots HC_2H$ and leading to HC_5N has also been suggested for the UV-irradiated acetylene/cyanoacetylene mixture in a cryogenic matrix.[34]

$$HC_3N\cdots HC_2H + h\nu \rightarrow HC_5N + H_2 \quad (8)$$

The equivalent of reactions (7) or (8) can also be envisioned to lead to formation of HC_9N:

$$HC_5N\cdots HC_5N + h\nu \rightarrow HC_9N + CN^{\bullet} + H^{\bullet} \quad (9)$$

$$HC_5N\cdots HC_4H + h\nu \rightarrow HC_9N + H_2 \quad (10)$$

The importance of precursors bound in a complex is rather unlikely for syntheses of chains longer than HC_5N. Experiments leading to formation of HC_7N showed no IR spectroscopic traces of such complexes, regardless of whether HC_3N+C_4H_2 or HC_5N+C_2H_2 mixtures were used.[36] The same is true for the present experiment using HC_5N and C_4H_2. In addition, experiments using HC_5N as a sole precursor did not result in the appearance of HC_9N (this argument, however, should be treated with caution, given that conditions were not optimized for the detection of HC_9N).

Reaction (6) would conclude an overall two-photon process (one photon for each radical to form). The generated radicals need to be in close physical proximity to one another for chain elongation to occur. Such a process was observed in the case of NC_6N (dicyanodiacetylene) formation from HC_3N, where the production rate increased with irradiation time during the initial stages of the photolysis. This increase demonstrates that $C_3N^{\bullet}$ radicals first needed to be created in sufficient concentration (*i.e*. sufficiently close to one another) before they could begin to recombine.[35] Our measurements (Figure 2) show that the HC_9N production rate decreases with irradiation time suggesting that the radical recombination mechanism (6) does not occur to any great extent.

One last processes that has not yet been discussed involves precursor molecules excited to a high electronic level, rather than dissociating into a free radical. If such excitation is occurring, it could not be distinguished from a radical path with the presently reported experiments.

CONCLUSIONS

UV-driven synthesis of HC_9N in a solid rare gas matrix, *via* coupling of HC_5N and C_4H_2, does occur. The targeted molecule, obtained here in amounts too small for producing measurable IR absorption signals, could be detected due to its strong phosphorescence, observed here for the first time. Experimentally derived spectroscopic characteristics are in a good accordance with

theoretical predictions. Phosphorescence excitation spectra gave insight to excited singlet electronic states, unattainable with standard UV absorption measurements. The forbidden $\tilde{B}\ ^1\Delta$ – $\tilde{X}\ ^1\Sigma^+$ system (rendered detectable due to coupling with a π–symmetry vibration) is well understood, while the analysis of fully allowed $\tilde{E}\ ^1\Sigma^+$ – $\tilde{X}\ ^1\Sigma^+$ and $\tilde{H}\ ^1\Sigma^+$ – $\tilde{X}\ ^1\Sigma^+$ transitions, entangled with forbidden transitions, requires further studies.

The described results are in agreement with previous reports on photochemical generation of similar but smaller molecules[34–36] in inert cryogenic matrices and suggest the validity of the adopted approach for the synthesis and spectral studies of even longer unsaturated carbon-nitrogen chains. In particular, the spectral origin of phosphorescence of a linear $HC_{11}N$ can be safely predicted. The cryogenic environment proved soft enough to adapt its structure during the synthesis of an approximately 1.2 nm long HC_9N molecule from precursors themselves too large to occupy single trapping sites (approx. 0.4 nm wide) of the *fcc*-type krypton lattice. It would be interesting to go a step further and find out whether it is possible to synthesize $HC_{11}N$ within a similar scheme.

Apart from HC_9N, we have observed other luminescing products in the described experiments, such as $C_{10}N_2$ (to be described separately), some of which remain unassigned. Further spectroscopic work on matrix isolated $HC_{2n+1}N$ species may lead to the detection of their isomers (in particular: isonitriles) and, as pointed out by the referee of this paper, possibly also to new insertion compounds $HRgC_{2n+1}N$, where Rg stands for Kr or Xe atoms. [74-75]

SUPPORTING INFORMATION

Calculated IR frequencies and intensities in accessible electronic states; visualization of vibrational modes in selected electronic states; phosphorescence excitation spectra of HC_7N and HC_9N.

ACKNOWLEDGMENT

This work was financially supported by the Polish National Science Centre, project no. 2011/03/B/ST4/02763, French-Polish scientific cooperation programs *Partenariat Hubert-Curien Polonium* (2012-2013) and *PICS* (2014-2016). U.S. is a beneficiary of the French Government scholarship *Bourse Eiffel*, managed by Campus France, and of the project "Scholarships for PhD students of Podlaskie Voivodeship". The project is co-financed by European Social Fund, Polish Government and Podlaskie Voivodeship. J.-C.G. thanks the Centre National d'Etudes Spatiales (CNES) and the French program Physique et Chimie du Milieu Interstellaire (PCMI) funded by the Conseil National de la Recherche Scientifique (CNRS) and CNES for financial support. Thanks are also due to Prof. Tomonari Wakabayashi for sharing his data on electronic absorption of HC_9N.

REFERENCE LIST

(1) Turner, B. E. Detection of Interstellar Cyanoacetylene. *Astrophys. J. Lett.* **1971**, *163*, L35.

(2) Dickinson, D. F. Detection of Cyanoacetylene at 18 GHz. *Astrophys. Lett.* **1972**, *12*, 235–236.

(3) McGee, R. X.; Balister, M.; Newton, L. M. Interstellar Cyanoacetylene − J=2→1, J=4→3 Transitions. *Mon. Not. R. Astron. Soc.* **1977**, *180* (4), 585–592.

(4) Gardner, F. F.; Winnewisser, G. Observations of the J = 1→0 Transitions of the ^{13}C Isotopic Species of Cyanoacetylene (HCCCN) in the Direction of Sagittarius B2. *Astrophys. J.* **1975**, *197*, L73.

(5) Mauersberger, R.; Henkel, C.; Sage, L. J. Dense Gas in Nearby Galaxies. III - HC_3N as an Extragalactic Density Probe. *Astron. Astrophys.* **1990**, *236*, 63–68.

(6) Kunde, V. G.; Aikin, A. C.; Hanel, R. A.; Jennings, D. E.; Maguire, W. C.; Samuelson, R. E. C_4H_2, HC_3N and C_2N_2 in Titan's Atmosphere. *Nature* **1981**, *292* (5825), 686–688.

(7) Coustenis, A. The Atmospheric Structure of Titan from Voyager to Cassini. *AGU Spring Meet. Abstr.* **2007**, *44*.

(8) Bockelée-Morvan, D.; Lis, D. C.; Wink, J. E.; Despois, D.; Crovisier, J.; Bachiller, R.; Benford, D. J.; Biver, N.; Colom, P.; Davies, J. K.; et al. New Molecules Found in Comet C/1995 O1 (Hale-Bopp). Investigating the Link between Cometary and Interstellar Material. *Astron. Astrophys.* **2000**, *353*, 1101–1114.

(9) Snell, R. L.; Schloerb, F. P.; Young, J. S.; Hjalmarson, A.; Friberg, P. Observations of HC_3N, HC_5N, and HC_7N in Molecular Clouds. *Astrophys. J.* **1981**, *244*, 45–53.

(10) Broten, N. W.; Oka, T.; Avery, L. W.; MacLeod, J. M.; Kroto, H. W. The Detection of HC_9N in Interstellar Space. *Astrophys. J.* **1978**, *223*, L105.

(11) Bell, M. B.; Avery, L. W.; MacLeod, J. M.; Matthews, H. E. The Excitation Temperature of HC_9N in the Circumstellar Envelope of IRC + 10216. *Astrophys. J.* **1992**, *400*, 551–555.

(12) Truong-Bach; Graham, D.; Nguyen-Q-Rieu. HC_9N from the Envelopes of IRC+10216 and CRL:2688. *Astron. Astrophys.* **1993**, *277*, 133.

(13) Bell, M. B.; Feldman, P. A.; Kwok, S.; Matthews, H. E. Detection of $HC_{11}N$ in IRC + 10°216. *Nature* **1982**, *295* (5848), 389–391.

(14) Bell, M. B.; Feldman, P. A.; Travers, M. J.; McCarthy, M. C.; Gottlieb, C. A.; Thaddeus, P. Detection of $HC_{11}N$ in the Cold Dust Cloud TMC-1. *Astrophys. J. Lett.* **1997**, *483* (1), L61.

(15) Loomis, R. A.; Shingledecker, C. N.; Langston, G.; McGuire, B. A.; Dollhopf, N. M.; Burkhardt, A. M.; Corby, J.; Booth, S. T.; Carroll, P. B.; Turner, B.; et al. Non-Detection of $HC_{11}N$ towards TMC-1: Constraining the Chemistry of Large Carbon-Chain Molecules. *Mon. Not. R. Astron. Soc.* **2016**, *463* (4), 4175–4183.

(16) Cherchneff, I.; Glassgold, A. E. The Formation of Carbon Chain Molecules in IRC +10216. *Astrophys. J. Lett.* **1993**, *419*, L41.

(17) Cherchneff, I.; Glassgold, A. E.; Mamon, G. A. The Formation of Cyanopolyyne Molecules in IRC + 10216. *Astrophys. J.* **1993**, *410*, 188–201.

(18) Woon, D. E.; Herbst, E. Quantum Chemical Predictions of the Properties of Known and Postulated Neutral Interstellar Molecules. *Astrophys. J. Suppl. Ser.* **2009**, *185* (2), 273.

(19) Botschwina, P.; Horn, M. Accurate Equilibrium Structure and Electric Dipole Moment of HC_9N: Predictions on the Basis of Large-Scale Coupled Cluster Calculations. *J. Mol. Spectrosc.* **1997**, *185* (1), 191–193.

(20) Thaddeus, P.; McCarthy, M. C. Carbon Chains and Rings in the Laboratory and in Space. *Spectrochim. Acta. A. Mol. Biomol. Spectrosc.* **2001**, *57* (4), 757–774.

(21) Boyd, R. J.; Jones, W. E.; Ling, K. W. Geometries, Energies and Polarities of Cyanopolyynes. *Chem. Phys.* **1981**, *58* (2), 203–210.

(22) Qi, J. Y.; Chen, M. D.; Wu, W.; Zhang, Q. E.; Au, C. T. Parity Alternation of Interstellar Molecules Cyanopolyynes HC_nN (n = 1–17). *Chem. Phys.* **2009**, *364* (1–3), 31–38.

(23) Vichietti, R. M.; Haiduke, R. L. A. The Infrared Fundamental Intensities of Some Cyanopolyynes. *Spectrochim. Acta. A. Mol. Biomol. Spectrosc.* **2012**, *90*, 1–11.

(24) Vichietti, R. M.; Haiduke, R. L. A Theoretical Systematic Study of a Series of Isocyanopolyynes. *Spectrochim. Acta. A. Mol. Biomol. Spectrosc.* **2013**, *114*, 197–204.

(25) Iida, M.; Ohshima, Y.; Endo, Y. Laboratory Detection of HC_9N Using a Fourier Transform Microwave Spectrometer. *Astrophys. J.* **1991**, *371*, L45.

(26) McCarthy, M. C.; Levine, E. S.; Apponi, A. J.; Thaddeus, P. Experimental Structures of the Carbon Chains HC_7N, HC_9N, and $HC_{11}N$ by Isotopic Substitution. *J. Mol. Spectrosc.* **2000**, *203* (1), 75–81.

(27) Kroto, H. W.; Heath, J. R.; Obrien, S. C.; Curl, R. F.; Smalley, R. E. Long Carbon Chain Molecules in Circumstellar Shells. *Astrophys. J.* **1987**, *314*, 352–355.

(28) Schermann, G.; Grösser, T.; Hampel, F.; Hirsch, A. Dicyanopolyynes: A Homologuous Series of End-Capped Linear Sp Carbon. *Chem. – Eur. J.* **1997**, *3* (7), 1105–1112.

(29) Cataldo, F. Polyynes and Cyanopolyynes: Their Synthesis with the Carbon Arc Gives the Same Abundances Occurring in Carbon-Rich Stars. *Orig. Life Evol. Biospheres* **2006**, *36* (5–6), 467–475.

(30) Cataldo, F. Monocyanopolyynes from a Carbon Arc in Ammonia: About the Relative Abundance of Polyynes Series Formed in a Carbon Arc and Those Detected in the Circumstellar Shells of AGB Stars. *Int. J. Astrobiol.* **2006**, *5* (01), 37–45.

(31) Wakabayashi, T.; Saikawa, M.; Wada, Y.; Minematsu, T. Isotope Scrambling in the Formation of Cyanopolyynes by Laser Ablation of Carbon Particles in Liquid Acetonitrile. *Carbon* **2012**, *50* (1), 47–56.

(32) Forte, G.; D'Urso, L.; Fazio, E.; Patanè, S.; Neri, F.; Puglisi, O.; Compagnini, G. The Effects of Liquid Environments on the Optical Properties of Linear Carbon Chains Prepared by Laser Ablation Generated Plasmas. *Appl. Surf. Sci.* **2013**, *272*, 76–81.

(33) Devienne, F. M.; Barnabé, C.; Ourisson, G. Synthesis of Further Biological Compounds in Interstellar-like Conditions. *Comptes Rendus Chim.* **2002**, *5* (10), 651–653.

(34) Coupeaud, A.; Kołos, R.; Couturier-Tamburelli, I.; Aycard, J. P.; Piétri, N. Photochemical Synthesis of the Cyanodiacetylene HC_5N: A Cryogenic Matrix Experiment. *J. Phys. Chem. A* **2006**, *110* (7), 2371–2377.

(35) Crépin, C.; Turowski, M.; Ceponkus, J.; Douin, S.; Boyé-Péronne, S.; Gronowski, M.; Kołos, R. UV-Induced Growth of Cyanopolyyne Chains in Cryogenic Solids. *Phys. Chem. Chem. Phys. PCCP* **2011**, *13* (37), 16780–16785.

(36) Couturier-Tamburelli, I.; Piétri, N.; Crépin, C.; Turowski, M.; Guillemin, J.-C.; Kołos, R. Synthesis and Spectroscopy of Cyanotriacetylene (HC_7N) in Solid Argon. *J. Chem. Phys.* **2014**, *140* (4), 044329.

(37) Turowski, M.; Crépin, C.; Douin, S.; Kołos, R. Formation and Spectroscopy of Dicyanotriacetylene (NC_8N) in Solid Kr. *J. Phys. Chem. A* **2014**.

(38) Trolez, Y.; Guillemin, J.-C. Synthesis and Characterization of 2,4-Pentadiynenitrile—A Key Compound in Space Science. *Angew. Chem. Int. Ed.* **2005**, *44* (44), 7224–7226.

(39) Khlifi, M.; Paillous, P.; Delpech, C.; Nishio, M.; Bruston, P.; Raulin, F. Absolute IR Band Intensities of Diacetylene in the 250 - 4300 cm^{-1} Region: Implications for Titan's Atmosphere. *J. Mol. Spectrosc.* **1995**, *174*, 116–122.

(40) Parr, R. G.; Weitao, Y. *Density-Functional Theory of Atoms and Molecules*; Oxford University Press, 1989.

(41) Bauernschmitt, R.; Ahlrichs, R. Treatment of Electronic Excitations within the Adiabatic Approximation of Time Dependent Density Functional Theory. *Chem. Phys. Lett.* **1996**, *256* (4), 454–464.

(42) Casida, M. E.; Jamorski, C.; Casida, K. C.; Salahub, D. R. Molecular Excitation Energies to High-Lying Bound States from Time-Dependent Density-Functional Response Theory: Characterization and Correction of the Time-Dependent Local Density Approximation Ionization Threshold. *J. Chem. Phys.* **1998**, *108* (11), 4439–4449.

(43) Stratmann, R. E.; Scuseria, G. E.; Frisch, M. J. An Efficient Implementation of Time-Dependent Density-Functional Theory for the Calculation of Excitation Energies of Large Molecules. *J. Chem. Phys.* **1998**, *109* (19), 8218–8224.

(44) Perdew, J. P.; Ziesche, P.; Eschrig, H. *Electronic Structure of Solids' 91*; Akademie Verlag, Berlin, 1991; Vol. 11.

(45) Perdew, J. P.; Chevary, J. A.; Vosko, S. H.; Jackson, K. A.; Pederson, M. R.; Singh, D. J.; Fiolhais, C. Atoms, Molecules, Solids, and Surfaces: Applications of the Generalized Gradient Approximation for Exchange and Correlation. *Phys. Rev. B* **1992**, *46* (11), 6671–6687.

(46) Perdew, J. P.; Chevary, J. A.; Vosko, S. H.; Jackson, K. A.; Pederson, M. R.; Singh, D. J.; Fiolhais, C. Erratum: Atoms, Molecules, Solids, and Surfaces: Applications of the

Generalized Gradient Approximation for Exchange and Correlation. *Phys. Rev. B* **1993**, *48* (7), 4978–4978.

(47) Perdew, J. P.; Burke, K.; Wang, Y. Generalized Gradient Approximation for the Exchange-Correlation Hole of a Many-Electron System. *Phys. Rev. B* **1996**, *54* (23), 16533–16539.

(48) Becke, A. D. Density□functional Thermochemistry. III. The Role of Exact Exchange. *J. Chem. Phys.* **1993**, *98* (7), 5648–5652.

(49) Yanai, T.; Tew, D. P.; Handy, N. C. A New Hybrid Exchange–Correlation Functional Using the Coulomb-Attenuating Method (CAM-B3LYP). *Chem. Phys. Lett.* **2004**, *393* (1–3), 51–57.

(50) Dunning, T. H. J. Gaussian Basis Sets for Use in Correlated Molecular Calculations. I. The Atoms Boron through Neon and Hydrogen. *J. Chem. Phys.* **1989**, *90* (2), 1007–1023.

(51) Kendall, R. A.; Jr, T. H. D.; Harrison, R. J. Electron Affinities of the First□row Atoms Revisited. Systematic Basis Sets and Wave Functions. *J. Chem. Phys.* **1992**, *96* (9), 6796–6806.

(52) Andersson, M. P.; Uvdal, P. New Scale Factors for Harmonic Vibrational Frequencies Using the B3LYP Density Functional Method with the Triple-ζ Basis Set 6-311+G(d,p). *J. Phys. Chem. A* **2005**, *109* (12), 2937–2941.

(53) Merrick, J. P.; Moran, D.; Radom, L. An Evaluation of Harmonic Vibrational Frequency Scale Factors. *J. Phys. Chem. A* **2007**, *111* (45), 11683–11700.

(54) Foresman, J. B.; Head-Gordon, M.; Pople, J. A.; Frisch, M. J. Toward a Systematic Molecular Orbital Theory for Excited States. *J. Phys. Chem.* **1992**, *96* (1), 135–149.

(55) Frisch, M. J.; Trucks, G. W.; Schlegel, H. B.; Scuseria, G. E.; Robb, M. A.; Cheeseman, J. R.; Scalmani, G.; Barone, V.; Mennucci, B.; Petersson, G. A.; et al. *Gaussian 09*; Gaussian, Inc.: Wallingford, CT, USA, 2009.

(56) *Jmol: An Open-Source Java Viewer for Chemical Structures in 3D.* http://www.jmol.org/

(57) *GABEDIT 2.4.8*, Allouche, A.-R. Gabedit--a Graphical User Interface for Computational Chemistry Softwares. *J. Comput. Chem.* **2011**, *32* (1), 174–182.

(58) *Chemcraft - Graphical Program for Visualization of Quantum Chemistry Computations,* http://chemcraftprog.com/; Andrienko G.A.; *Chemcraft 1.8 (build 180)*.

(59) *Dalton, a Molecular Electronic Structure Program,* Release 2.0 (2005), See http://www.kjemi.uio.no/software/dalton/dalton.html; C. Angeli, K. L. Bak, V. Bakken, O. Christiansen, R. Cimiraglia, S. Coriani, P. Dahle, E. K. Dalskov, T. Enevoldsen, B. Fernandez, et al..

(60) Christiansen, O.; Koch, H.; Jørgensen, P. The Second-Order Approximate Coupled Cluster Singles and Doubles Model CC2. *Chem. Phys. Lett.* **1995**, *243* (5), 409–418.

(61) Christiansen, O.; Koch, H.; Halkier, A.; Jørgensen, P.; Helgaker, T.; Merás, A. S. de. Large□scale Calculations of Excitation Energies in Coupled Cluster Theory: The Singlet Excited States of Benzene. *J. Chem. Phys.* **1996**, *105* (16), 6921–6939.

(62) Hald, K.; Hättig, C.; Jørgensen, P. Triplet Excitation Energies in the Coupled Cluster Singles and Doubles Model Using an Explicit Triplet Spin Coupled Excitation Space. *J. Chem. Phys.* **2000**, *113* (18), 7765–7772.

(63) Job, V. A.; King, G. W. The Electronic Spectrum of Cyanoacetylene: Part II. Analysis of the 2300-Å System. *J. Mol. Spectrosc.* **1966**, *19* (1–4), 178–184.

(64) Bruston, P.; Poncet, H.; Raulin, F.; Cossart-Magos, C.; Courtin, R. UV Spectroscopy of Titan's Atmosphere, Planetary Organic Chemistry, and Prebiological Synthesis: I. Absorption Spectra of Gaseous Propynenitrile and 2-Butynenitrile in the 185- to 250-nm Region. *Icarus* **1989**, *78* (1), 38–53.

(65) Kołos, R. *Carbon-Nitrogen Chain Molecules in the Laboratory and in Interstellar Medium*; Institute of Physical Chemistry of the Polish Academy of Sciences: Warsaw, 2003.

(66) Turowski, M.; Crépin, C.; Gronowski, M.; Guillemin, J.-C.; Coupeaud, A.; Couturier-Tamburelli, I.; Piétri, N.; Kołos, R. Electronic Absorption and Phosphorescence of Cyanodiacetylene. *J. Chem. Phys.* **2010**, *133* (7), 074310.

(67) Vuitton, V.; Gée, C.; Raulin, F.; Bénilan, Y.; Crépin, C.; Gazeau, M.-C. Intrinsic Lifetime of Metastable Excited C_4H_2: Implications for the Photochemistry of C_4H_2 in Titan's Atmosphere. *Planet. Space Sci.* **2003**, *51* (13), 847–852.

(68) Anderson, B. D.; Gordon, C. M. The Laser Synthesis of Linear Polyynes: The Particle in a Box Revisited. *J. Chem. Educ.* **2008**, *85* (9), 1279.

(69) Maier, J. P. Electronic Spectroscopy of Carbon Chains. *J. Phys. Chem. A* **1998**, *102* (20), 3462–3469.

(70) Turowski, M.; Gronowski, M.; Boyé-Péronne, S.; Douin, S.; Monéron, L.; Crépin, C.; Kołos, R. The C_3N^- Anion: First Detection of Its Electronic Luminescence in Rare Gas Solids. *J. Chem. Phys.* **2008**, *128* (16), 164304.

(71) Turowski, M. Niskotemperaturowe Badania Fotochemii I Spektroskopii Cyjanoacetylenów O Znaczeniu Astrofizycznym. PhD Dissertation, Institute of Physical Chemistry, Polish Academy of Sciences: Warsaw, 2012.

(72) Szczepaniak, U. Spectroscopy and Photochemistry of Astrophysically Relevant Molecules of the Cyanoacetylene Family. PhD Dissertation, Institute of Physical Chemistry, Polish Academy of Sciences; Universite Paris-Sud, Universite Paris-Saclay: Warsaw, 2017.

(73) Gronowski, M. TD-DFT Benchmark: Excited States of Atoms and Atomic Ions. *Comput. Theor. Chem.* **2017**, *1108*, 50–56.

(74) Khriachtchev, L.; Lignell, A.; Tanskanen, H.; Lundell, J.; Kiljunen, H.; Räsänen, M. Insertion of Noble Gas Atoms into Cyanoacetylene: An ab Initio and Matrix Isolation Study. *J. Phys. Chem. A* **2006**, *110*, 11876-11885.

(75) Turowski, M.; Gronowski, M.; Guillemin, J.C-.; Kołos, R. Generation of H-Kr-C_5N and H-Xe-C_5N molecules. *J. Mol. Struct.* **2012**, *1025*, 140-146.

TOC Graphic

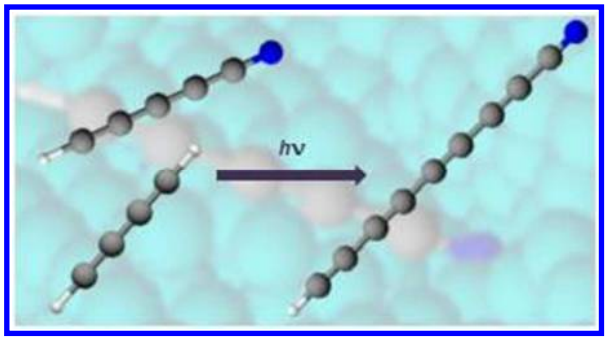

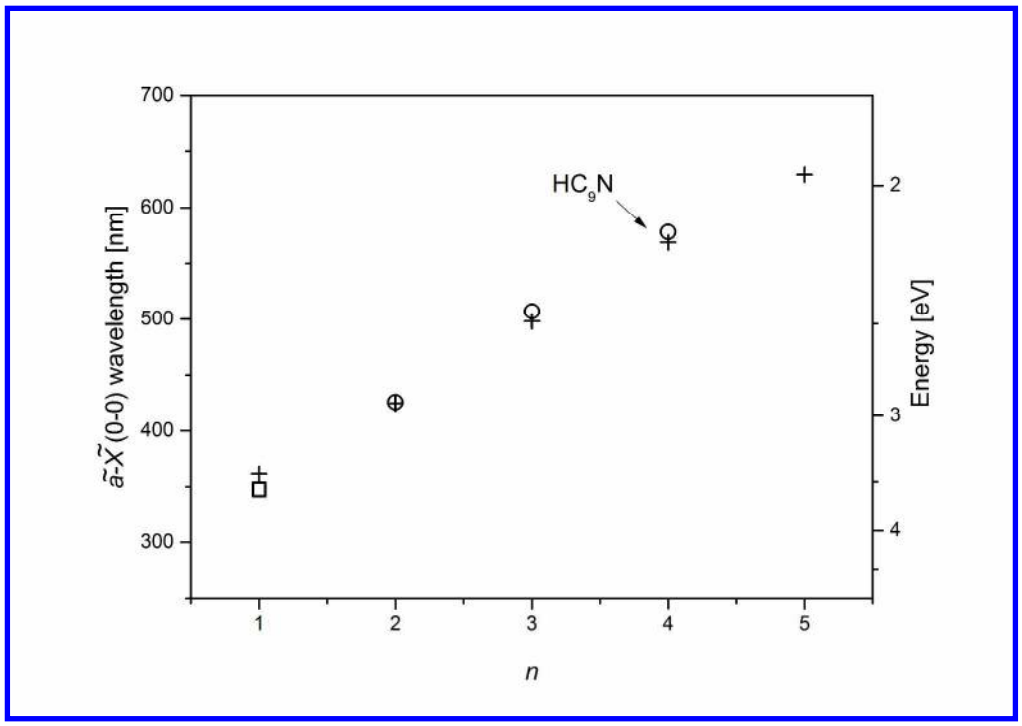

Phosphorescence origin wavelength as a function of carbon chain length for HC2n+1N molecules. Circles mark the experimental values for Kr matrices (HC3N does not phosphoresce; value observed for the isoelectronic C3N– anion70 is entered for n=1 as an open square). Crosses correspond to CAM-B3LYP/aug-cc-pVTZ predictions. Experimental data for HC5N and HC7N come from Refs. 37,66.

289x203mm (300 x 300 DPI)